Effect of tensile stress on the behavior of Iron-Silicon single crystal: magnetization, magnetostriction and magnetic Barkhausen noise

Eric Wasniewski, Laurent Daniel, Mathieu Domenjoud, Patrick Fagan, Fan Zhang, Benjamin Ducharne

Effect of tensile stress on the behavior of Iron-Silicon single crystal: magnetization, magnetostriction and magnetic Barkhausen noise

Eric Wasniewski, Laurent Daniel, Mathieu Domenjoud, Patrick Fagan, Fan Zhang and Benjamin Ducharne

Abstract—**This study investigates the magneto-elastic behavior of Iron-Silicon single crystals with predetermined crystallographic orientations. For that purpose, multi-crystalline samples with a large single-crystal in their central area were cut from a large-grain high-permeability electrical steel. The samples were subjected to tensile stress. Three complementary characterization techniques were employed to explore the effect of stress on the magnetization mechanisms: classical hysteresis loops to analyze the global magnetic response, magnetic Barkhausen noise measurements to study local magnetic domain dynamics and pinning effects, and magnetostriction measurements to quantify strain behavior and shed light on the magneto-elastic coupling. The comparative analysis reveals the intricate relationships between magnetic and mechanical properties, emphasizing the role of microstructural features such as crystallographic orientation in the magnetization process.**

These findings can help in the definition of optimal non-destructive testing (NDT) conditions for stress observation. For instance, the accumulation of magnetic Barkhausen noise energy up to saturation is revealed as a promising indicator for indirectly assessing stress in ferromagnetic materials.

Index Terms—**Domain wall motion, Magnetic Barkhausen noise energy, Magneto-mechanical characterization, Non-destructive testing, Rotational magnetization**

I. Introduction

UNDERSTANDING magnetization mechanisms in ferromagnetic materials is essential for advancing fundamental research and industrial applications [1]. In automotive, power generation, manufacturing, electronics, and healthcare industries, a precise knowledge of these mechanisms is critical to achieving specific technological goals. For example, in electric vehicles [2], optimizing the magnetization process in motor cores can reduce energy losses, enhancing vehicle range and battery life. In power generation, transformers and wind turbine generators use electrical steels, where controlling domain wall motion and minimizing eddy currents are essential for maximizing energy efficiency and managing heat [3, 4]. Manufacturing processes and infrastructure maintenance rely on magnetic non-destructive testing (NDT) methods like Magnetic Flux Leakage (MFL) and Eddy Current Testing (ECT) to identify surface and internal defects in pipelines, rail tracks, and structural steels [5, 6]. The accurate interpretation of these tests demands an in-depth understanding of magnetization mechanisms to detect cracks, corrosion, and other potential failure causes. Electronics and telecommunications use ferrite materials in components such as Radio Frequency filters and transformers [7-9], where optimizing magnetic permeability and reducing losses at high frequencies is crucial for reliable signal transmission and reduced electromagnetic interference. In healthcare, Magnetic Resonance Imaging scanners use ferromagnetic materials to generate strong, stable magnetic fields. Advances in magnetic hyperthermia for cancer treatment rely on ferromagnetic nanoparticles whose magnetization must be precisely controlled to target and heat tumor cells without damaging surrounding tissue [10, 11]. All these examples highlight how a detailed understanding of magnetization mechanisms enables industries to refine material properties to meet stringent technical requirements, from energy efficiency to defect detection and medical precision.

The magnetization behavior of magnetic materials results from a combination of complex, localized mechanisms, primarily 180° and non-180° domain wall motion, and magnetization rotation [12, 13]. These mechanisms govern domain orientation and evolution under various external conditions. Describing these fundamental processes is essential in evaluating how external factors, particularly mechanical stress, impact magneto-mechanical properties in ferromagnetic materials. Stress sensitivity in these materials, as largely documented [14-17], arises from the influence of stress on each of these distinct mechanisms. However, due to their intertwined nature, isolating the effects of stress on an individual mechanism remains challenging [18].

To unravel this complexity, this study investigates the effect of tensile stress on iron-silicon (FeSi 3% wt) single crystals, which serve as a model material for exploring magnetization mechanisms. Using single crystals eliminates complexities associated with grain boundaries and texture effects in polycrystalline materials [19]. This advantage enables a more precise correlation between macroscopic magneto-elastic

Eric Wasniewski and Fan Zhang are with CETIM, 60300 Senlis, France. Eric Wasniewski, Laurent Daniel, Mathieu Domenjoud and Patrick Fagan are with Université Paris-Saclay, Centrale Supelec, CNRS, Laboratoire de Génie Electrique et Electronique de Paris, 91192, Gif-sur-Yvette, France and with Sorbonne Université, CNRS, Laboratoire de Génie Electrique et Electronique de Paris, 75252, Paris, France.

Benjamin Ducharne is with ELyTMaX IRL3757, CNRS, Univ. Lyon, INSA Lyon, Centrale Lyon, Universite Claude Bernard Lyon 1, Tohoku University, Sendai, Japan, and with Univ Lyon, INSA-Lyon, LGEF EA682, F69621, France. Corresponding author: benjamin.ducharne@insa-lyon.fr.

response and intrinsic magnetization mechanisms. Furthermore, FeSi 3% single crystals exhibit high permeability and low coercivity, making them suitable for isolating and understanding the primary factors influencing magnetization under mechanical stress [20, 21].

Three major macroscopic measurements will be used: the magnetization hysteresis curve $B_a(H_{surf})$, the magnetostriction curve $\varepsilon^{\mu}(H_{surf})$, and the Magnetic Barkhausen Noise (MBN). Focusing on these three responses aims to elucidate the influence of mechanical stress on magnetization mechanisms. Indeed, while the magnetization curve reflects all magnetization mechanisms, magnetostriction curves are insensitive to 180° domain wall motion. It highlights the contributions of non-180° domain wall motion and magnetization rotation [22]. On the other hand, MBN is hardly sensitive to magnetization rotation. It is a good indicator of the role of 180° and non-180° domain wall motion.

TABLE I
MAGNETIZATION MECHANISMS FOR EACH MEASUREMENT TECHNIQUES

		Measurement technique		
		B-H loop	Magnetostriction	MBN energy
Magnetization mechanism	180° wall motion	X		X
	Non-180° wall motion	X	X	X
	Magnetization rotation	X	X	

The measurements were performed under various tensile stress levels and for different magnetic excitation angles with respect to the crystal orientation. This approach allows an examination of how stress impacts domain wall motion and magnetization rotation and how these effects depend on the direction of magnetic excitation. Combining these characterization results provides a multi-faceted understanding of the interplay between mechanical and magnetic properties in FeSi single crystals and, more generally, ferromagnetic materials.

II. Tested Specimens, Experimental Conditions And Analysis

2.1 – Specimens

The tested specimens are obtained from grain-oriented (GO) FeSi 3% laminations thermally treated to induce grains of exceptional size (> several cm) [23, 24]. They were supplied by ThyssenKrupp (Isbergues, France). Their thickness δ is 0.3 mm. The formation of large grains results in superior magnetic anisotropy and reduced core losses. In this material, a strong crystallographic texture with easy axes <100> aligned with the rolling direction (RD) enables efficient magnetization along this direction [25, 26]. Fig. 1 depicts one of the specimens. A large grain (length ≈ 60 mm) is visible in the central part.

The laminations of GO FeSi 3% were cut by electrical discharge machining to avoid residual stress altering the magnetic properties.

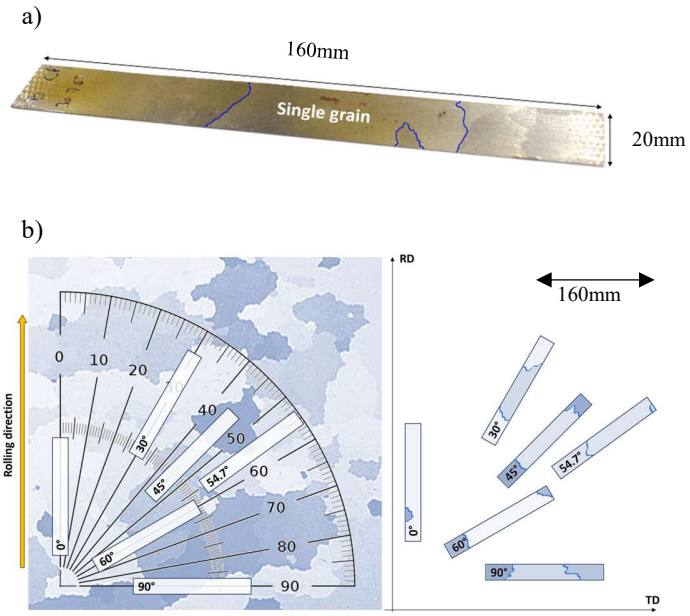

Fig. 1.a) Picture and dimensions of a tested specimen. **Fig. 1.b)** Tested specimens and their orientations.

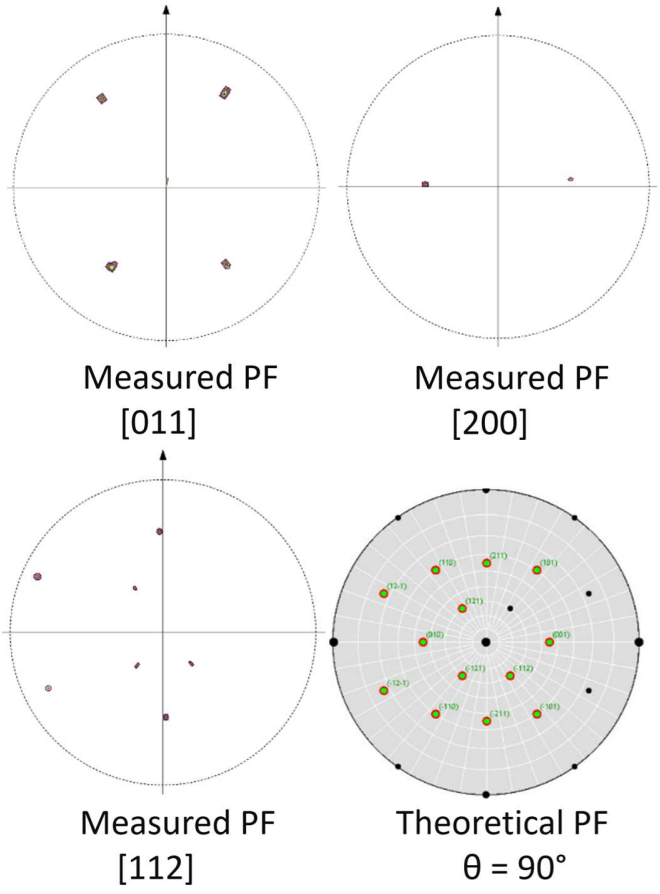

Fig. 2. Pole figures (PF) for a specimen oriented at θ = 90°.

A series of specimens were cut at θ = 0, 30, 45, 54.7, 60, and 90°, where θ = 0° and 90° are the rolling (RD) and the transverse (TD), respectively (see Fig. 1 for illustration). While RD contains mostly <100> directions, TD mostly contains <110> directions [27], and <111> directions can be found at θ ≈ 54.7°. Four specimens were prepared for each angle. The anticipated crystallographic orientation was confirmed using X-ray diffraction, with an angular deviation of less than 1°. Fig. 2 illustrates, for example, the pole figures obtained for one sample at θ = 90°.

2.2 – Experimental setups

To ensure the reproducibility and consistency of the experimental results, two independent experimental setups were used, both designed to measure the $B_a(H_{surf})$ curves under identical conditions [28, 29] (See Appendix, for illustration). Furthermore, the first setup, setup A in Fig. 3, was optimized for recording the MBN signals (high sampling frequency).

TABLE II
DETAILED FEATURES FOR EACH EXPERIMENTAL SETUP

	Left – setup A	Right – setup B [28, 29]
Tension-compression machine	Shimadzu, autograph AGS-X with a 100 kN load cell ADS-100kNX (Japan)	Zwick Roell Z030 with a 30 kN load cell Xforce P (Germany)
Frequency generator	A 3210A Agilent (USA)	DS 1006 dSPACE processor board (Germany)
Power amplifier	Kikusui PCR2000WEA - I_{MAX} = 20 A and U_{MAX} = 200 V with 0.1% accuracy (Japan)	Kepco BOP 72-14MG - I_{MAX} = 14 A and U_{MAX} = 72 V with 0.2% accuracy (Korea)
Acquisition card	Dewesoft Sirius (Slovenia)	DS 1006 dSPACE processor board (Germany)
H_{surf} measurement	Through electrical current measurement	Projekt Elektronic Hall Effect Sensor & Gaussmeter FM 302 (Germany)

The second, setup B in Fig. 3, was used for magnetostriction measurements.

Moreover, the reliability of the findings was verified by comparing the results on magnetization curves obtained from these complementary setups. The magnetization curves obtained from setup A will only be presented in detail to avoid repetition. In [30-32], the stress dependence of magnetic properties was analyzed by varying the magnetization angle relative to the stress direction, resulting in a cos² dependence of the magnetic parameters. In contrast, in our study, the mechanical stress and hysteresis measurements were performed along the same direction, with specimens cut at different angles relative to the rolling direction.

A. Mechanical stress

Tension-compression machines and the associated material testing operation software were used for the stress application. The series of measurements were done by increasing incrementally (ΔF = 250 N / $\Delta\sigma$ = 50 MPa) the mechanical force up to F_{MAX} = 1000 N (σ_{MAX} = 200 MPa) to remain below the yield strength of the tested specimens (330 – 380 MPa). At each step, the stress remained constant throughout the magnetic measurement process and monitored by the load cell with a precision of ±1%.

B. Magnetic excitation

The magnetic circuit is made of two U-shaped GO FeSi 3% yokes, ensuring the closure of the magnetic flux. The tested specimen was placed and kept inside the testing machine thanks to a diamagnetic fixture (see picture in Fig. 3).

A series circuit of two primary coils, one wound around each yoke (N_t = 500 turns each), was supplied in current by a power amplifier to ensure magnetic field excitation.

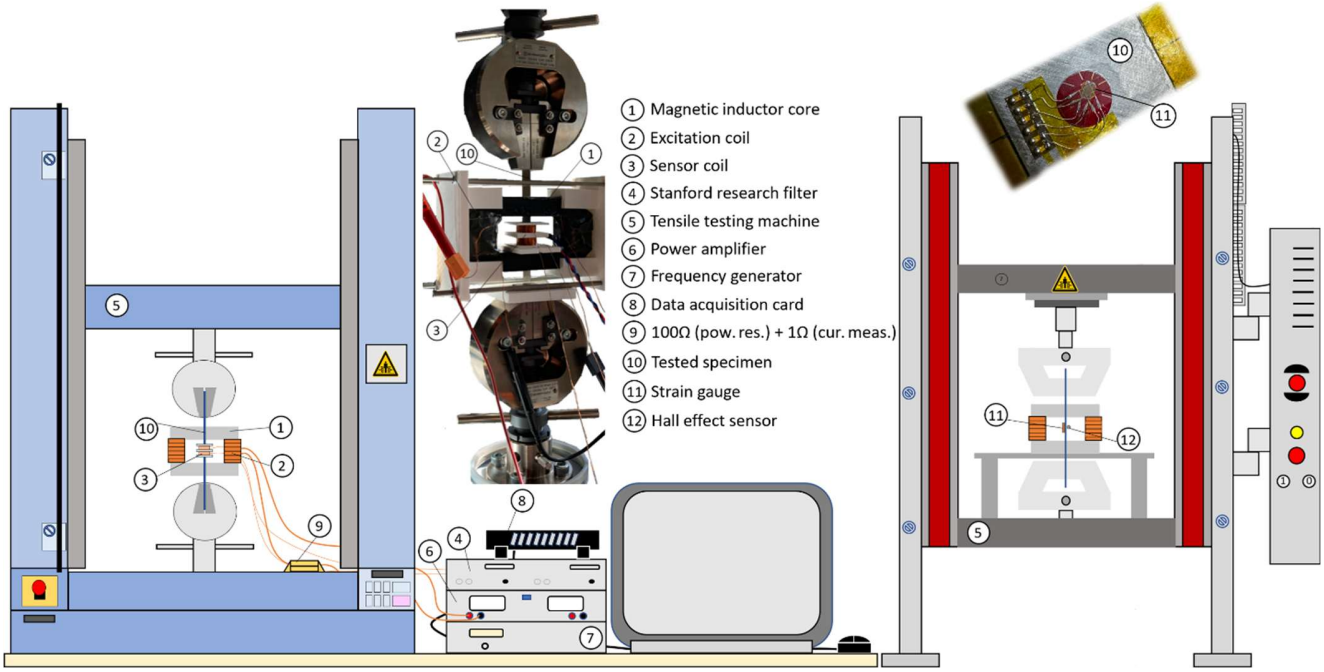

Fig. 3. 2D sketches and pictures of the experimental setups. Left: Setup A; Right: Setup B.

A waveform generator was used to obtain a sinusoidal current waveform at 0.1 Hz.

The cumulative cross-section of the yokes is 6 10^{-4} m^2, which is at least 100 times larger than the tested specimens' cross-section. Considering this geometrical difference, the yokes' equivalent reluctance was assumed negligible, and H_{surf} was supposed to be entirely confined in the tested specimens. In setup A, an R = 100 Ω power resistor was plugged in series with the excitation coils. This resistor was large enough to ensure that the amplifier voltage and current $I(t)$ outputs had similar waveforms, regardless of the working conditions. Another R = 1 Ω resistor was plugged in series to monitor the current $I(t)$. Once measured, $I(t)$ was used to return the estimated field $H_{surf}(t)$, according to Eq. (1):

$$H_{surf}(t) = \frac{2N_t I(t)}{L_e} \quad (1)$$

L_e = 40 mm is the length of the specimen in the tested area. For setup B, a gaussmeter was used to directly measure $H_{surf}(t)$ at the surface of the specimen.

C. Magnetic measurements (MBN, B_a)

Two N = 200-turns wrapped coil sensors plugged in series opposition were positioned around the central single crystalline area for the MBN measurement. This configuration effectively cancels out common-mode signals, such as induced voltages from the applied field (including the low-frequency component at the excitation frequency) and external electromagnetic noise, thereby isolating the MBN signal generated by domain wall dynamics [33]. Preliminary tests with movable sensor coils showed that, as long as the coils were positioned away from the grain boundaries, the distance between them had a limited impact. To ensure consistency in comparisons, this distance was kept constant throughout the experimental process.

The sensor coil raw electromotive force was filtered and amplified using a Stanford Research SR650 (Sunnyvale, CA, USA). The cut-off frequencies were set to 0.5 kHz and 15 kHz, and the gain to 40 dB per decade. All the signals were recorded with a Dewesoft (Trbovlje, Slovenia) Sirius data acquisition card. The square, the integration (Eq. (2)), and a drift correction were done numerically using Matlab® software. All the data were averaged over four excitation periods to reduce parasitic noises.

In parallel, the induced electromagnetic force Ø(t) coming from one of the wrapped coils only was used to calculate $B_a(t)$ (Eq. (2)):

$$B_a(t) = \frac{1}{N_t S}\int \emptyset(t)dt \quad (2)$$

The tested specimen cross-section is S = 6 10^{-6} m^2.

The wrapped coils configuration, by enhancing the detection of high-frequency components of the Barkhausen noise spectrum, emphasizes local domain wall activity. While this reduces sensitivity to long-range correlations influenced by demagnetizing fields, it is beneficial in our context, as it provides spatially resolved information. The resulting signal is thus predominantly representative of the studied single crystal, with negligible contributions from neighboring grains due to the combination of frequency content and spatial attenuation.

D. Magnetostriction measurements (ε^{μ})

The longitudinal and transverse strains, $\varepsilon^{\mu}_{//}$ and $\varepsilon^{\mu}_{\perp}$ respectively, were obtained using a strain rosette gauge (FRA-3-11, Tokyo Measuring Instruments Laboratory, Tokyo, Japan) mounted on all tested specimens' faces. The gauges were connected to a strain gauge conditioner–amplifier (2120B, Vishay Measurements Group, Toronto, Canada). The reference state is the demagnetized state under pre-stress. All measurement signals were acquired using the same data acquisition card.

E. Data analysis

A moving average of 10-point was applied to a dataset of 50000 points per period, in post-processing to smooth the magnetostriction measurements. Additionally, to facilitate comparison with $B_a(H_{surf})$ and $MBN_{energy}(H_{surf})$, the magnetostriction, which is typically plotted as a function of the magnetization (M), was instead plotted as a function of the magnetic field H_{surf}.

2.3 – Magnetic Barkhausen noise energy

During the magnetization process, MBN is generated from domain walls' encounters and interactions with microstructural features in ferromagnetic materials. These defects act as pinning sites, causing the domain wall to stop momentarily and jump [34, 35].

These abrupt movements result in rapid local changes in the magnetic flux, which, in turn, produces the MBN. MBN is essentially the sum of these individual magnetic events. Mechanical stress changes the distribution and dynamics of magnetic domains, therefore impacting the MBN signal [36, 37].

The practical computation of the MBN_{energy} [38, 39] involves three steps:

_ To monitor the MBN signal under the form of an electrical voltage: $e(t)$ (see Fig. 4, step 1).

_ To square the MBN signal: $e^2(t)$ and multiply it by the sign of the magnetic excitation time derivative (see Fig. 4, step 2).

_ To time integrate the product of the sign of the magnetic excitation time derivative and the square of the MBN signal (see Fig. 4, step 3) :

$$MBN_{energy}(t) = \int_0^t sign\left(\frac{dH_{surf}}{ds}\right) e^2(s)ds \quad (3)$$

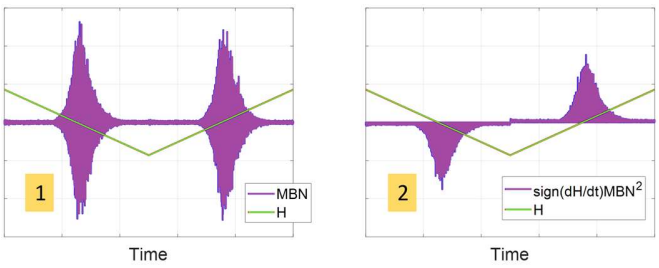

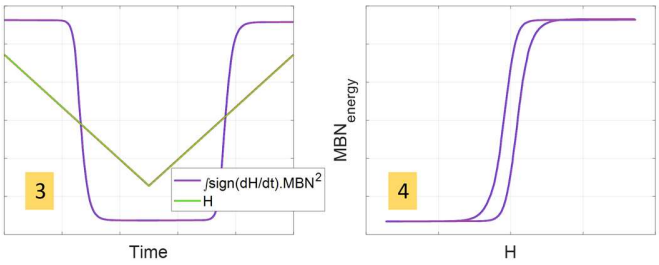

Fig. 4. $MBN_{energy}(H_{surf})$ hysteresis loop, construction process.

From this concept of the MBN_{energy}, the $MBN_{energy}(H_{surf})$ hysteresis cycles can be defined, depicting how MBN_{energy} changes with respect to the external magnetizing field H_{surf} (see Fig. 4, step 4). This representation shows the MBN_{energy} on the y-axis and H_{surf} on the x-axis [39]. The resulting cycles provide additional information about the magnetization process, especially compared to classical magnetization loops $B_a(H_{surf})$, where B_a is the flux density averaged through the specimen cross-section. More precisely, it can help to establish the respective contributions of domain wall motion and magnetization rotation during the magnetization process. Previous works [38] revealed similarities between MBN_{energy} and classical hysteresis loops for grain-oriented electrical steel (GO FeSi) but significant differences for iron-cobalt (FeCo) laminations. These differences were interpreted as a limited contribution of magnetization rotation for GO FeSi in contrast to a substantial contribution for FeCo. Still, most of these results are qualitative and based on experimental observations. They lack theoretical confirmation, especially considering that MBN is sensitive to many parameters, including residual stress, dislocation density, grain size, and microstructural defects.

Prior to each measurement series, the integrator drift caused by background electronic noise was determined by recording the sensor output in the absence of magnetic excitation. This baseline drift was then subtracted from the measured signal during post-processing to ensure accurate estimation of the Barkhausen noise energy. Additional tests were conducted throughout the experimental campaign to monitor any variation in this drift, and corrections were applied when necessary to maintain consistency across all measurements.

2.4 – Magnetostriction

A ferromagnetic domain is defined as a region of the crystal characterized by a uniform magnetization $\overrightarrow{M^{\alpha}}$ with amplitude M_S and a uniform magnetostriction strain $\varepsilon_{\alpha}^{\mu}$. For a cubic system, the magnetostriction tensor of a ferromagnetic domain α is defined by:

$$\varepsilon_{\alpha}^{\mu} = \frac{3}{2}\begin{pmatrix} \lambda_{100}(\gamma_1^2 - \frac{1}{3}) & \lambda_{111}\gamma_1\gamma_2 & \lambda_{111}\gamma_1\gamma_3 \\ \lambda_{111}\gamma_1\gamma_2 & \lambda_{100}(\gamma_2^2 - \frac{1}{3}) & \lambda_{111}\gamma_2\gamma_3 \\ \lambda_{111}\gamma_1\gamma_3 & \lambda_{111}\gamma_2\gamma_3 & \lambda_{100}(\gamma_3^2 - \frac{1}{3}) \end{pmatrix} \quad (4)$$

Eq. (4) expresses the magnetostriction strain tensor in the crystallographic coordinate system, where γ_i are the direction cosines of the magnetization $\overrightarrow{M^{\alpha}}$. The magnetostrictive constants λ_{100} and λ_{111} are material parameters equal to λ_{100} = 23 10^{-6} and λ_{100} = -4.5 10^{-6} for FeSi 3%. Magnetostriction measurements characterize the strain response of a ferromagnetic material under an applied magnetic field, providing insights into the magneto-elastic coupling. Specifically, they help quantify the contributions of non-180° domain wall motion and magnetization rotation, as 180° domain wall motion does not produce magnetostrictive strain. In [19], Rizzo *et al.* proposed an analysis of domain microstructure evolution based on the measurement of magnetization and magnetostriction in single crystals, which were obtained similarly to those in this study. In our study, the magnetostriction curves ($\varepsilon^{\mu}(H_{surf})$) provide essential information on how tensile stress influences domain distribution, domain wall dynamics and magnetization processes, particularly highlighting stress-dependent reorientation effects.

III. Experimental Results

As mentioned in sub-section 2.2, $B_a(H_{surf})$ measurements were performed on both experimental setups to check consistency.

The results showed good agreement. Therefore, only the dataset for $B_a(H_{surf})$ curve from setup A is presented hereafter. An example of the MBN raw data has been presented in the appendix fig 10., which shows the raw data of the sample 0°, 54,7° and 90° with a with an offset to make reading easier. Experimental results for θ = 0, 54.7, and 90° are shown in Fig. 5-7 below. Results at θ = 30, 45, and 60° can be found in the appendix in Fig. 11-13.

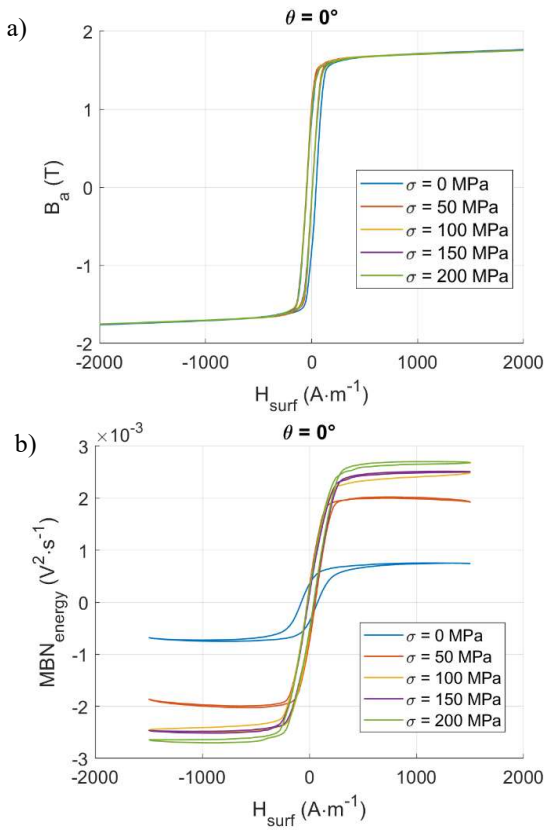

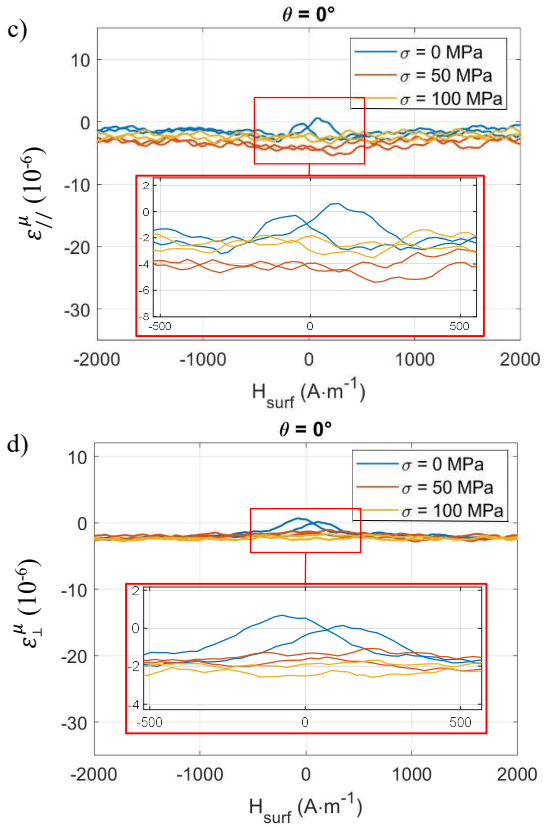

Fig. 5a. $B_a(H_{surf})$. **Fig. 5b.** $MBN_{energy}(H_{surf})$. **Fig. 5c.** $\varepsilon^{\mu}_{//}(H_{surf})$. **Fig. 5d.** $\varepsilon^{\mu}_{\perp}(H_{surf})$ cycles for θ = 0° and different levels of uniaxial tensile stress.

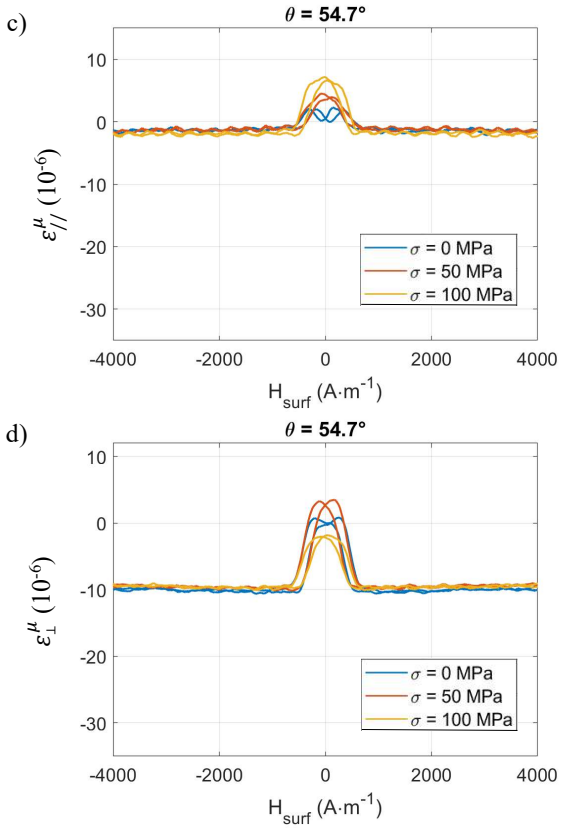

Fig. 6a. $B_a(H_{surf})$. **Fig. 6b.** $MBN_{energy}(H_{surf})$. **Fig. 6c.** $\varepsilon^{\mu}_{//}(H_{surf})$. **Fig. 6d.** $\varepsilon^{\mu}_{\perp}(H_{surf})$ cycles for θ = 54.7° and different levels of uniaxial tensile stress.

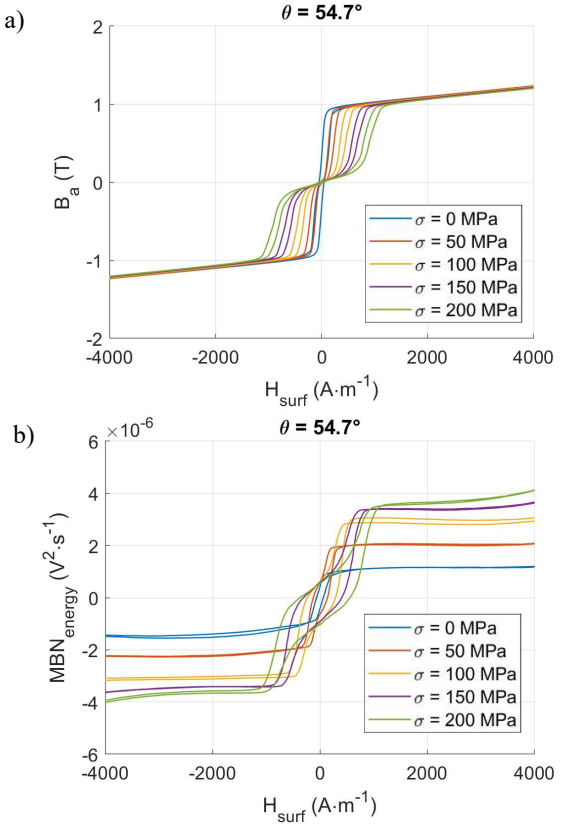

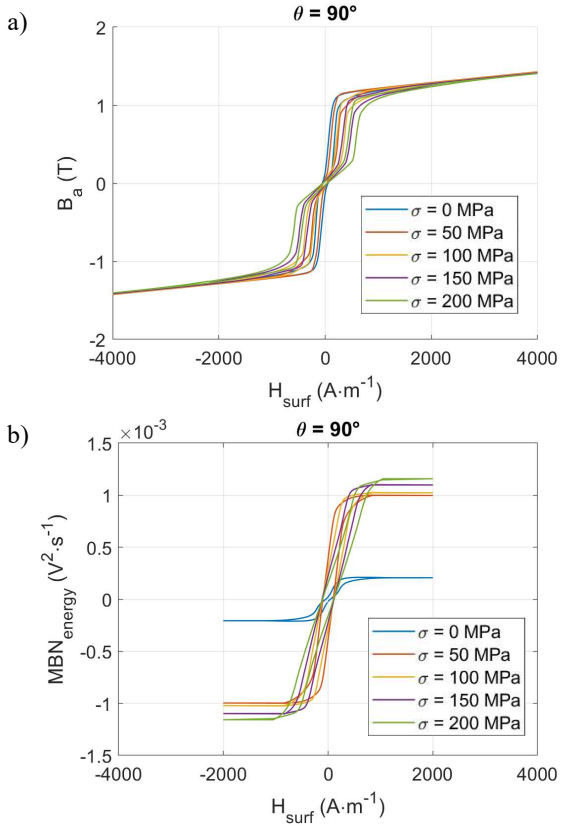

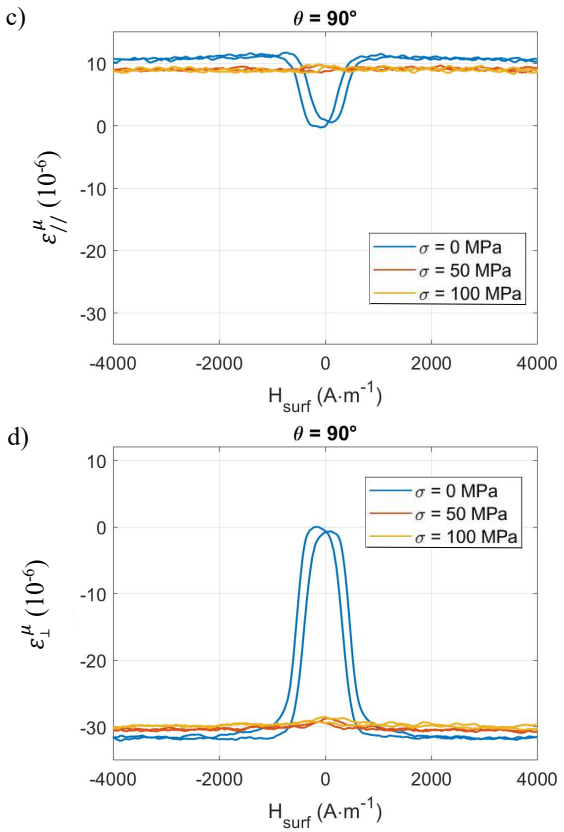

Fig. 7a. $B_a(H_{surf})$. **Fig. 7b.** $MBN_{energy}(H_{surf})$. **Fig. 7c.** $\varepsilon^{\mu}_{//}(H_{surf})$. **Fig. 7d.** $\varepsilon^{\mu}_{\perp}(H_{surf})$ cycles for θ = 90° and different levels of uniaxial tensile stress.

The magnetostrictive curves are presented only up to 100 MPa, as the effect of stress saturates, and no further change is observed beyond this point (unless the yield stress is reached).

IV. Discussion

At first glance, it is apparent that the majority of the magnetostriction curves (Fig. 5-7) align well with those reported in the literature for polycrystalline grain-oriented GO FeSi 3% specimens [19, 40-43].

Applied tensile stress plays a critical role in magnetostriction variations, which are primarily influenced by non-180° domain wall motion and magnetization rotation. At low field levels, magnetization is dominated by domain wall motion. At higher field levels, it is predominantly driven by magnetization rotation.

The effect of tension stress on these mechanisms depends on its orientation relative to the applied magnetic field, as it can either facilitate or hinder them. Non-180° domain wall motions also generate Barkhausen noise.

However, it is challenging to isolate the Barkhausen noise associated with non-180° domain wall activity from that of 180° domain walls, despite the expectation that 180° domain wall motion occurs at a slower speed and is associated with lower-frequency Barkhausen noise [44].

Significant differences are observed between the $MBN_{energy}(H_{surf})$ and the $B_a(H_{surf})$ cycles. These differences include the absence of variation in the $MBN_{energy}(H_{surf})$ cycles once the loop closes in the saturated region. In contrast, for the same level of magnetic excitation, B_a keeps increasing in the $B_a(H_{surf})$ cycles due to the magnetization rotation mechanism. This effect has been previously documented in the literature [18, 38].

A detailed analysis of the magnetization process for each value of θ is provided below:

_ At θ = 0°, magnetostriction is absent, and while the effect of applied stress on the $B_a(H_{surf})$ cycles is limited, it is significant on the $MBN_{energy}(H_{surf})$ curves. The interpretation is that, under no applied stress, all domains are already aligned with both the applied stress direction and the magnetic field. Consequently, no non-180° domain wall motion or magnetization rotation occurs during the magnetization process, which is only driven by 180° domain wall motion. This stress-dependent motion generates no magnetostriction strain and has a limited effect on the overall magnetization.

_ At θ = 30° and 45°, a small level of magnetostriction is observed at low field levels, primarily attributed to non-180° domain wall motion. At higher field levels, the impact of magnetization rotation becomes apparent, reflecting a uniform variation in magnetostriction that increases and decreases at a constant rate. This effect is also noticeable in the comparison between the $B_a(H_{surf})$ and $MBN_{energy}(H_{surf})$ curves, with an increase in B_a and no variation of the MBN_{energy} in the high field range. This stress-dependent effect requires a higher field amplitude to become evident under higher stress levels. In the low-field range, the impact of stress on the 180° domain wall motions, previously observed at θ = 0°, is also perceptible.

_ At θ = 60° and 90°, magnetostriction exhibits pronounced variations without applied stress. Magnetic domains initially oriented in the rolling direction significantly reorganize toward the transverse direction, inducing considerable non-180° domain wall motion and, hence, magnetostriction. This effect is less pronounced under applied stress, where the stress facilitates transverse alignment, reducing non-180° domain wall activity and consequently reducing magnetostriction in the longitudinal direction. In the θ = 90° configuration, the theoretical strain, based on the magnetostriction tensor (Eq. (8)) and the domain family distribution predictions (as reported in [19]) is $\Delta\varepsilon^{\mu}_{//} = 3/4\ \lambda_{100} \approx 17\ 10^{-6}$ and $\Delta\varepsilon^{\mu}_{\perp} = -\ 3/2\ \lambda_{100} \approx -34\ 10^{-6}$, which aligns well with the experimental measurements.

_ At θ = 54.7°, in the absence of stress, the longitudinal strain exhibits an increasing positive deformation at low fields (-500 A·m^{-1} < H_{surf} < 500 A·m^{-1}), probably due to non-180° domain wall motions, which are the first to occur. Beyond this field range, the strain decreases due to the reduction of the non-180° domain wall activity (between 500 and 800 A·m^{-1}). Following this initial decrease, further reduction is observed, explained by magnetization rotation. Under applied stress, non-180° domain wall activity begins as soon as the magnetization process starts, facilitated by the application of stress. This observation confirms the intense domain wall activity observed by comparing the $B_a(H_{surf})$ and $MBN_{energy}(H_{surf})$ cycles, which shows a large coercivity difference. This property comes from

an irreversible reorganization of the magnetic domains, inducing no overall magnetization state change but domain wall motions and significant MBN activity. This effect is particularly important in the Rayleigh region at $\sigma = 200$ MPa of the $MBN_{energy}(H_{surf})$ cycle. In this configuration, the theoretical deformation is $\Delta\varepsilon_{//}^{\mu} = 0$ and $\Delta\varepsilon_{\perp}^{\mu} = -1/2.\ \lambda_{100} \approx -11\ 10^{-6}$, which again aligns well with the experimental results.

V. Sensitivity of Magnetic Indicators to Stress

As mentioned in the introduction, evaluating mechanical stress in structural ferromagnetic steel is essential for predicting undesired degradation and potential failure [45-47]. Section V highlighted the significant impact of mechanical stress on the magnetization mechanisms.

The MBN signature is well-suited for modern Non-Destructive Testing (NDT) applications due to its cost-effectiveness and minimal space requirements [48]. In [18], the reconstruction and analysis of $MBN_{energy}(H_{surf})$ were tested as tools for stress evaluation in polycrystalline materials.

This new study replicates this evaluation strategy. However, in the single crystalline configuration, where the experimental conditions are more constrained, the relationship between magnetization mechanisms and stress is simplified, making it easier to interpret.

In [18], the influence of stress was observed through four magnetic indicators read on the $MBN_{energy}(H_{surf})$ hysteresis cycle:

_ B_r: remanence,
_ $H_{surf\,c}$: coercivity,
_ A_{hys}: area of the hysteresis loop,
_ $H_{surf\,95}$: magnetic field measured at MBN_{energy} = 0.95 x max (MBN_{energy})
_ $H_{surf\,99}$: magnetic field measured at MBN_{energy} = 0.99 x max (MBN_{energy}).

(Although separated by only 4%, the difference between $H_{surf\,95}$ and $H_{surf\,99}$ is primarily associated with domain wall motions occurring in the highly saturated range (mostly 90° domain walls that are more difficult to trigger). Based on this observation, we supposed the influence of mechanical stress would be more pronounced).

The initial idea was to opt for the same indicators, but the noisy measurements in the saturation zone brought inaccurate results. Thus, $H_{surf\,95}$ and $H_{surf\,99}$ were replaced by MBN_{energy} at H_{surf} = 1000 A·m^{-1} and MBN_{energy} at H_{surf} = 2000 A·m^{-1}, respectively, which equally represented the MBN behavior close ($H_{surf\,95}$) or very close ($H_{surf\,99}$) to the saturation but in a much more stable and consistent way. These indicators have different values on the increasing or decreasing branch of the $MBN_{energy}(H_{surf})$ loop.

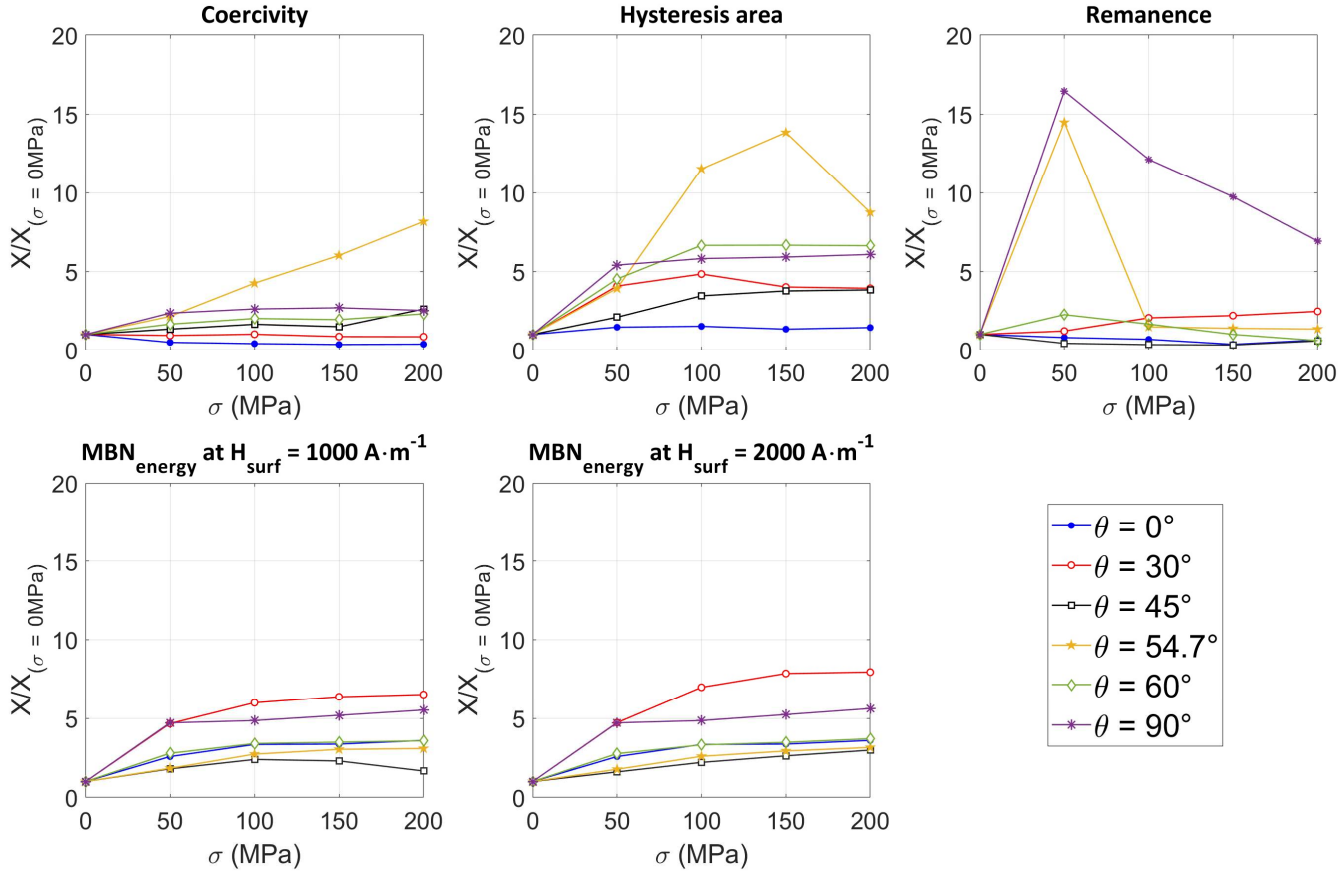

Fig. 8. Uniaxial tensile stress dependence of the magnetic indicators normalized by the corresponding stress-free reference.

Therefore, they were estimated based on the anhysteretic curve. The remanence $MBN_{energy\ r}$ was added to the pool of tested indicators.

Fig. 8 illustrates the evolution of these indicators as a function of applied tensile stress, normalized by their values at σ = 0 MPa. The most linearly stress-sensitive indicator is MBN_{energy} at H_{surf} = 2000 A·m^{-1}, which captures the cumulative effect of domain wall activity throughout the magnetization cycle. This strong correlation suggests that the parameter effectively reflects stress-induced alterations in domain wall dynamics.

The overall patterns observed in Fig. 8 can be explained by considering the competing effects of stress on non-180° and 180° domain wall motions. At low stress levels, domain wall displacement dominates, contributing significantly to MBN_{energy}. As stress increases, the energy required for domain wall motion rises, leading to a shift in the $MBN_{energy}(H_{surf})$ curve and an increase in coercivity. This shift is particularly pronounced in FeSi single crystals due to their well-defined anisotropic behavior. The consistent increase in MBN_{energy} at H_{surf} = 2000 A·m^{-1} suggests that this indicator integrates both low- and high-field domain wall contributions, making it a robust candidate for stress evaluation. Finally, all experimental MBN measurements were repeated using the surface sensor shown in Fig. 9a to explore our approach's validity in NDT conditions. The sensor consisted of a ferrite core in a rod shape, wrapped with a 1000-turn coil. The resulting variations of MBN_{energy} at H_{surf} = 2000 A·m^{-1} as a function of uniaxial stress σ are shown in Fig. 9b. The linear dependency between MBN_{energy} at H_{surf} = 2000 A·m^{-1} and σ appears even if it is less evident for θ = 54.7 and 60°. This initial test in NDT conditions will require further investigation.

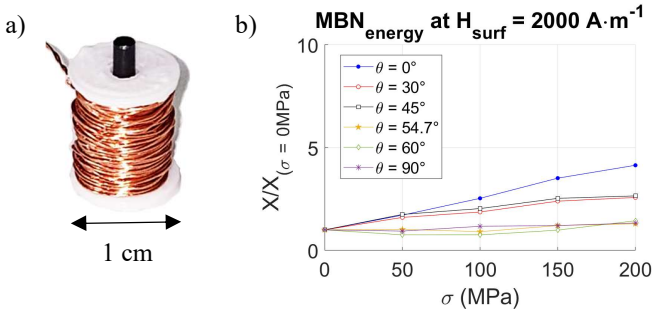

Fig. 9a. Picture of the MBN surface coil sensor. **Fig. 9b.** Uniaxial tensile stress dependence of the MBN_{energy} at H_{surf} = 2000 A·m^{-1} normalized by the corresponding stress-free reference.

VI. Conclusion

This study analyzes the magneto-elastic behavior of FeSi single crystals under various magnetic field intensities, stress conditions, and angles relative to the rolling direction. It provides insights into the interplay between magnetization, magnetostriction strain, magnetic Barkhausen noise, domain wall motion, and magnetization rotation.

Key findings confirm that magnetostriction behavior is strongly influenced by the misorientation between the magnetic field and the rolling direction and by the relative contributions of non-180° and 180° domain wall motions. The variation of magnetostriction across different angles θ emphasizes the complex dependency of magnetization processes on the angular orientation and intensity of the applied stress. For instance, at θ = 0°, the absence of magnetostriction aligns with theoretical expectations due to the lack of non-180° domain wall motion. In contrast, at higher angles (θ = 60° and 90°), significant magnetostriction arises, driven by large-scale domain wall reorganization and rotation, particularly in unstressed conditions. These effects diminish with stress application, reflecting the stress-induced facilitation of transverse alignment. The observations at θ = 54.7° underscore the nuanced role of non-180° domain wall activity and stress in governing magnetostriction strain, particularly in the Rayleigh region.

Magnetic Barkhausen Noise (MBN) characterization is a valuable non-destructive method for assessing internal mechanical stress in electrical steel laminations through surface measurements. However, the evaluation process is complex due to various factors that can similarly distort the MBN signal. MBN occurs locally within the ferromagnetic material and is consequently affected by the demagnetizing field but this impact is difficult to assess.

MBN_{energy} at saturation was already identified as the MBN indicator for observing tensile stress in polycrystalline grain-oriented FeSi laminates [18]. This work confirms this feature in single crystal conditions and across various magnetization orientations. Moreover, this indicator captures the entire magnetization cycle, making it less sensitive to experimental variations and suitable for industrial applications.

Future research should expand to different materials and mechanical stress conditions, such as compression and bi/tri-axial stresses.

References

[1] F. Fiorillo, G. Bertotti, C. Appino and M. Pasquale, 2016. Soft magnetic materials. In *Wiley Encyclopedia of Electrical and Electronics Engineering* (pp. 1-42). John Wiley & Sons, Inc.

[2] M. Kimiabeigi, J.D. Widmer, R. Long, Y. Gao, J. Goss, R. Martin, T. Lisle, J.S. Vizan, A. Michaelides and B. Mecrow, 2015. High-performance low-cost electric motor for electric vehicles using ferrite magnets. *IEEE Transactions on Industrial Electronics*, *63*(1), pp. 113-122.

[3] B.S. Ram, A.K. Paul and S.V. Kulkarni, 2021. Soft magnetic materials and their applications in transformers. *Journal of Magnetism and Magnetic Materials*, *537*, p. 168210.

[4] Y. Liu, M. Noe, J. Ou, P. Breining, M. Veigel and M. Doppelbauer, 2018. Measurement of magnetic materials at room and cryogenic temperature for their application to superconducting wind generators. *IEEE Transactions on Applied Superconductivity*, *28*(3), pp. 1-6.

[5] I. Tomas, 2004. Non-destructive magnetic adaptive testing of ferromagnetic materials. *Journal of magnetism and magnetic materials*, *268*(1-2), pp. 178-185.

[6] S. Zhang, B. Ducharne, S. Takeda, G. Sebald and T. Uchimoto, 2021. Identification of the ferromagnetic hysteresis simulation parameters using classic non-destructive testing equipment. *Journal of Magnetism and Magnetic Materials*, *531*, p. 167971.

[7] A. Goldman, 2006. *Modern ferrite technology*. Springer Science & Business Media.

[8] V. Tsakaloudi and V.T Zaspalis, 2007. A new Mn–Zn ferrite for high-speed data transmission applications in telecommunication networks. *Journal of magnetism and magnetic materials*, *310*(2), pp. 2540-2542.
[9] E. Roess, 1982. Soft magnetic ferrites and applications in telecommunication and power converters. *IEEE Transactions on Magnetics*, *18*(6), pp.1529-1534.
[10]D. Serantes, D. Baldomir, C. Martinez-Boubeta, K. Simeonidis, M. Angelakeris, E. Natividad, M. Castro, A. Mediano, D.X. Chen, A. Sanchez and L.I. Balcells, 2010. Influence of dipolar interactions on hyperthermia properties of ferromagnetic particles. *Journal of Applied Physics*, *108*(7), p. 073918.
[11]C.L. Dennis and R. Ivkov, 2013. Physics of heat generation using magnetic nanoparticles for hyperthermia. *International Journal of Hyperthermia*, *29*(8), pp. 715-729.
[12]G. Bertotti, 1998. *Hysteresis in magnetism: For physicists, materials scientists, and engineers*. Gulf Professional Publishing.
[13]R.M. Bozorth, 1993. *Ferromagnetism* , p. 992.
[14]D. Singh, P. Rasilo, F. Martin, A. Belahcen and A. Arkkio, 2015. Effect of mechanical stress on excess loss of electrical steel sheets. *IEEE Transactions on Magnetics*, *51*(11), pp. 1-4.
[15]E. Hristoforou and A. Ktena, 2007. Magnetostriction and magnetostrictive materials for sensing applications. *Journal of Magnetism and Magnetic Materials*, *316*(2), pp. 372-378.
[16]D.P. Bulte, R.A. Langman, 2002. Origins of the magnetomechanical effect, *Journal of Magnetism and Magnetic Materials*, 251(2), pp. 229-243
[17]A. Ouazib, M. Domenjoud, P. Fagan, L. Daniel : Effect of tension and compression stress on the magnetic losses in a low-Carbon steel, IEEE Transactions on Magnetics, 60(9):2001105 (2024)
[18]P. Fagan, B. Ducharne, L. Daniel, A. Skarlatos, M. Domenjoud and C. Reboud, 2022. Effect of stress on the magnetic Barkhausen noise energy cycles: A route for stress evaluation in ferromagnetic materials. *Materials Science and Engineering: B*, *278*, p. 115650.
[19]K.J. Rizzo, O. Hubert and L. Daniel, 2010. Magnetic and magnetostrictive behavior of iron-silicon single crystals under uniaxial stress. *IEEE Transactions on Magnetics*, *46*(2), pp.270-273.
[20]S. Zhang, B. Ducharne, G. Sebald, S. Takeda and T. Uchimoto, 2023. Magnetic indicators for evaluating plastic strains in electrical steel: Toward non-destructive assessment of the magnetic losses. *NDT & E International*, *134*, p. 102780.
[21]O Perevertov and R Schäfer, Influence of applied tensile stress on the hysteresis curve and magnetic domain structure of grain-oriented Fe–3%Si steel, *J. Phys. D: Appl. Phys*. 47 (2014) 185001
[22]A.J. Moses, 1990. Electrical steels: past, present and future developments. *IEE Proceedings A (Physical Science, Measurement and Instrumentation)*, *137*(5), pp. 233-245.
[23]K. Koyama, T. Goto, T. Kanomata and R. Note, 1999. Precise magnetization measurements of single-crystalline FeSi under high pressure. *Journal of the Physical Society of Japan*, *68*(5), pp. 1693-1698.
[24]Z. Xia, Y. Kang and Q. Wang, 2008. Developments in the production of grain-oriented electrical steel. *Journal of Magnetism and Magnetic Materials*, *320*(23), pp.3229-3233.
[25]Y. Hayakawa, 2017. Mechanism of secondary recrystallization of Goss grains in grain-oriented electrical steel. *Science and Technology of advanced MaTerialS*, *18*(1), pp. 480-497.
[26]S. Birosca, A. Nadoum, D. Hawezy, F. Robinson and W. Kockelmann, 2020. Mechanistic approach of Goss abnormal grain growth in electrical steel: Theory and argument. *Acta Materialia*, *185*, pp. 370-381.
[27]A. Faba and S. Quondam Antonio, 2021. An overview of non-destructive testing of goss texture in grain-oriented magnetic steels. Mathematics, 9(13), p. 1539.
[28]M. Domenjoud, E. Berthelot, N. Galopin, R. Corcolle, Y. Bernard and L. Daniel, 2019. Characterization of giant magnetostrictive materials under static stress: influence of loading boundary conditions. *Smart Materials and Structures*, *28*(9), p. 095012.
[29]M. Domenjoud and L. Daniel, 2023. Effects of plastic strain and reloading stress on the magneto-mechanical behavior of electrical steels: Experiments and modeling. *Mechanics of Materials*, *176*, p 104510.
[30]O. Stupakov, T. Uchimoto and T. Takagi, 2010. Magnetic anisotropy of plastically deformed low-carbon steel. *Journal of Physics D: Applied Physics*, *43*(19), p.195003.
[31]O. Perevertov, 2007. Influence of the residual stress on the magnetization process in mild steel. *Journal of physics D: Applied physics*, *40*(4), p.949.
[32]T.W. Krause, L. Clapham, A. Pattantyus and D.L. Atherton, 1996. Investigation of the stress-dependent magnetic easy axis in steel using magnetic Barkhausen noise. *Journal of Applied Physics*, *79*(8), pp.4242-4252.
[33]P. Fagan, B. Ducharne, S. Zurek, M. Domenjoud, A. Skarlatos, L. Daniel and C. Reboud, 2022. Iterative methods for waveform control in magnetic measurement systems. *IEEE Transactions on Instrumentation and Measurement*, *71*, pp.1-13.
[34]H. Sakamoto, M. Okada and M. Homma, 1987. Theoretical analysis of Barkhausen noise in carbon steels. *IEEE transactions on magnetics*, *23*(5), pp. 2236-2238.
[35]P. Fagan, S. Zhang, G. Sebald, T. Uchimoto and B. Ducharne, 2023. Barkhausen noise hysteresis cycle: Theoretical and experimental understanding. *Journal of Magnetism and Magnetic Materials*, *578*, p. 170810.
[36]D. Atherton and D. Jiles, 1983. Effects of stress on the magnetization of steel. *IEEE Transactions on magnetics*, *19*(5), pp. 2021-2023.
[37]D.M. Stewart, K.J. Stevens and A.B. Kaiser, 2004. Magnetic Barkhausen noise analysis of stress in steel. *Current Applied Physics*, *4*(2-4), pp. 308-311.
[38]P. Fagan, B. Ducharne, L. Daniel and A. Skarlatos, 2021. Multiscale modelling of the magnetic Barkhausen noise energy cycles. *Journal of Magnetism and Magnetic Materials*, *517*, p. 167395.
[39]B. Ducharne, M.Q. Le, G. Sebald, P.J. Cottinet, D. Guyomar and Y. Hebrard, 2017. Characterization and modeling of magnetic domain wall dynamics using reconstituted hysteresis loops from Barkhausen noise. *Journal of Magnetism and Magnetic Materials*, *432*, pp. 231-238.
[40]A. Hubert and R. Schäfer, 2008. *Magnetic domains: the analysis of magnetic microstructures*. Springer Science & Business Media.
[41]O. Hubert and L. Daniel, 2008. Multiscale modeling of the magneto-mechanical behavior of grain-oriented silicon steels. *Journal of Magnetism and Magnetic Materials*, *320*(7), pp. 1412-1422.
[42]S. Ito, T. Mifune, T. Matsuo and C. Kaido, 2016. Energy-based magnetization and magnetostriction modeling of grain-oriented silicon steel under vectorial excitations. *IEEE Transactions on Magnetics*, *52*(5), pp. 1-4.
[43]H. Mogi, Y. Matsuo and T. Kumano, 1999. AC magnetostriction hysteresis and magnetization direction in grain-oriented silicon steel. *IEEE transactions on magnetics*, *35*(5), pp. 3364-3366.
[44]S. Chikazumi, 1997. *Physics of ferromagnetism*, 506. Oxford University Press.
[45]D.M. Stewart, K.J. Stevens and A.B. Kaiser, 2004. Magnetic Barkhausen noise analysis of stress in steel. *Current Applied Physics*, *4*(2-4), pp. 308-311.
[46]J. Anglada-Rivera, L.R. Padovese and J. Capo-Sanchez, 2001. Magnetic Barkhausen noise and hysteresis loop in commercial carbon steel: influence of applied tensile stress and grain size. *Journal of magnetism and magnetic materials*, *231*(2-3), pp. 299-306.
[47]L. Mierczak, D.C. Jiles and G. Fantoni, 2010. A new method for evaluation of mechanical stress using the reciprocal amplitude of magnetic Barkhausen noise. *IEEE Transactions on Magnetics*, *47*(2), pp. 459-465.
[48]B. Ducharne, G. Sebald, H. Petitpré, H. Lberni, E. Wasniewski and F. Zhang, 2023. Magnetic Signatures and Magnetization Mechanisms for Grinding Burns Detection and Evaluation. *Sensors*, *23*(10), p. 4955.
[49]S.K. Shekhawat, B. Vadavadagi, V.D. Hiwarkar, J. Dumbre, A. Ingle and I. Samajdar, 2012. Magnetic properties in deformed grain oriented electrical steel: On the role of strain hardening exponent and microstructural developments. ISIJ international, 52(11), pp.2100-2108.

APPENDIX

Additional figures

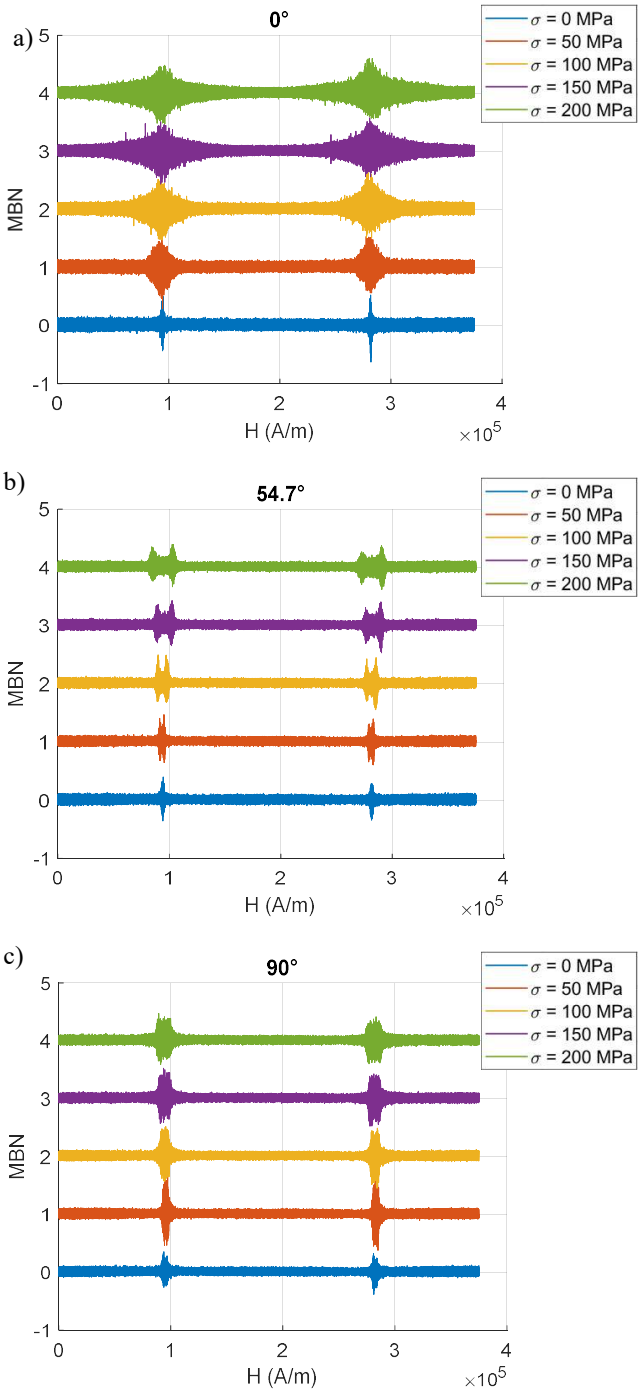

Fig. 10a. Raw MBN signal at 0° **Fig. 10b.** Raw MBN signal at 54,7° **Fig. 110.** Raw MBN signal at 90°

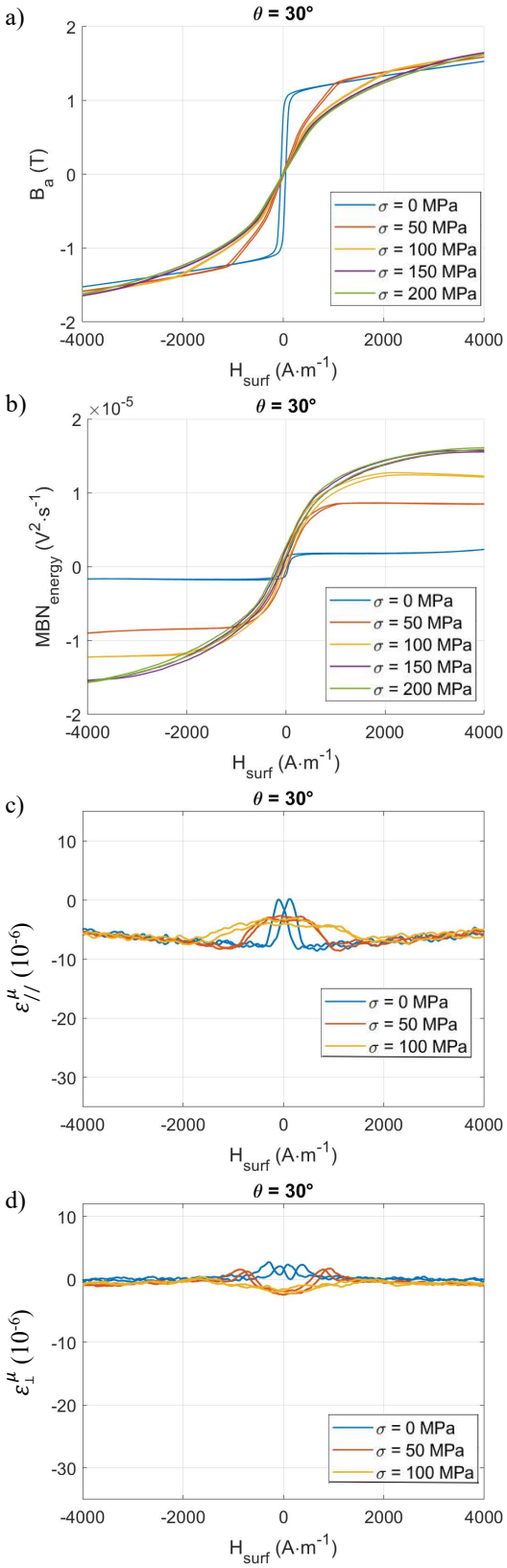

Fig. 11a. $B_a(H_{surf})$. **Fig. 11b.** $MBN_{energy}(H_{surf})$. **Fig. 11c.** $\varepsilon^{\mu}_{//}(H_{surf})$. **Fig. 11d.** $\varepsilon^{\mu}_{\perp}(H_{surf})$ cycles for θ = 30° and different levels of uniaxial tensile stress.

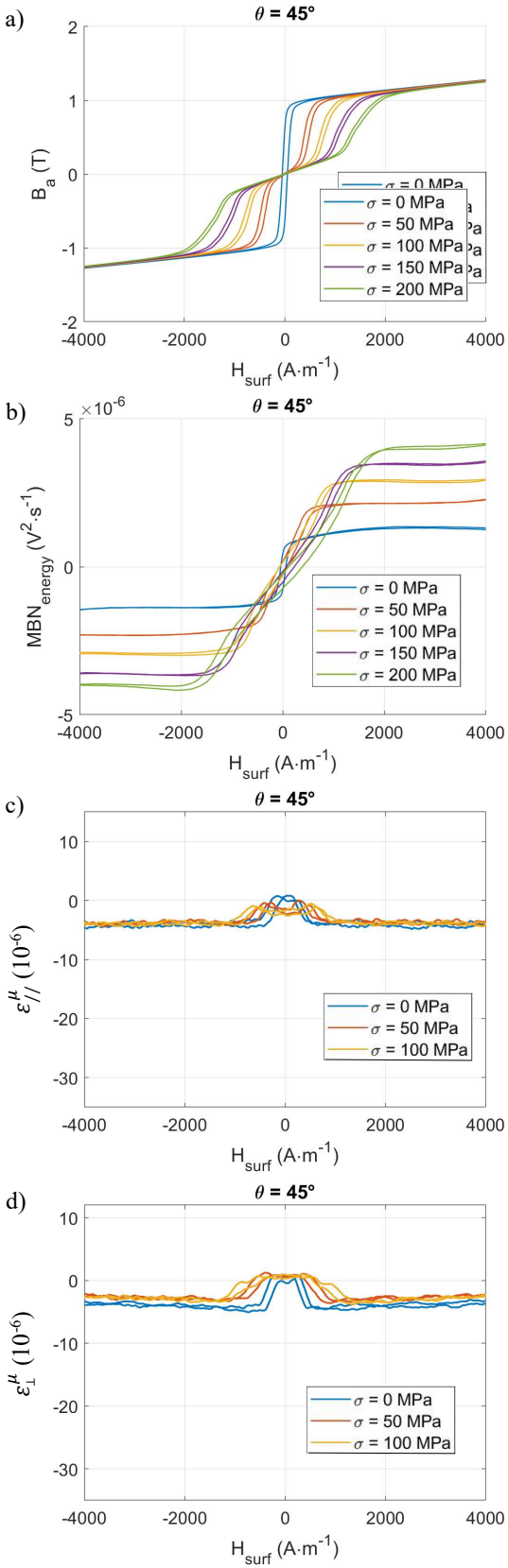

Fig. 12a. $B_a(H_{surf})$. **Fig. 12b.** $MBN_{energy}(H_{surf})$. **Fig. 12c.** $\varepsilon^{\mu}_{//}(H_{surf})$. **Fig. 12d.** $\varepsilon^{\mu}_{\perp}(H_{surf})$ cycles for θ = 45° and different levels of uniaxial tensile stress.

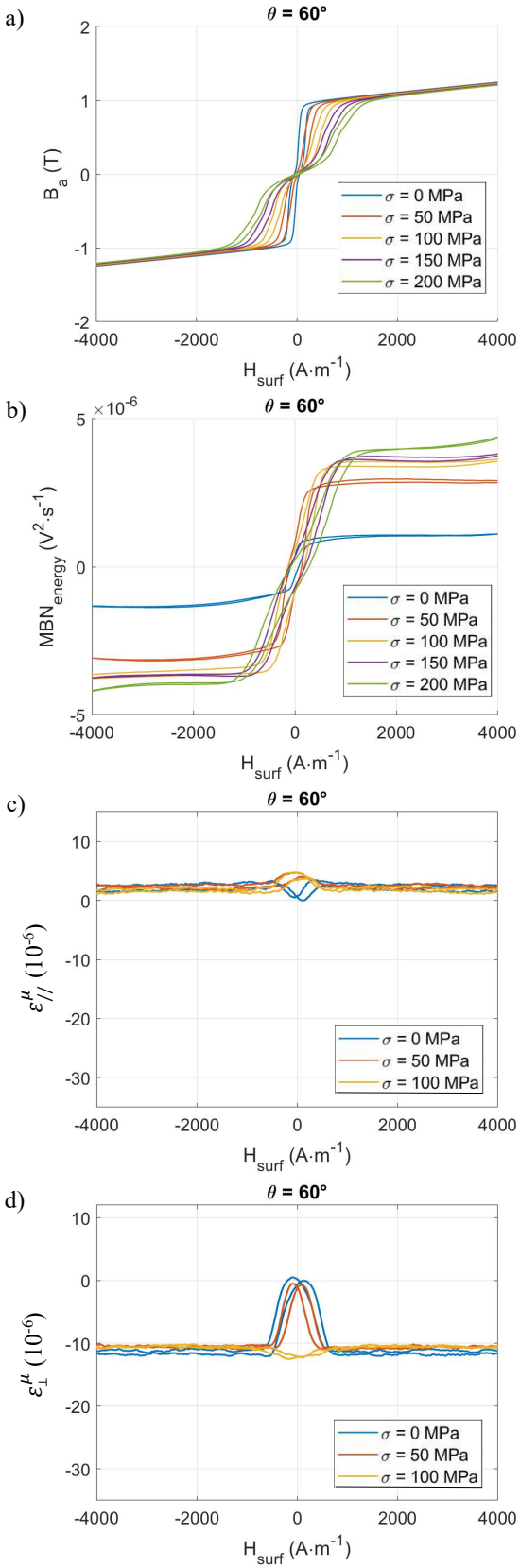

Fig. 13a. $B_a(H_{surf})$. **Fig. 13b.** $MBN_{energy}(H_{surf})$. **Fig. 13c.** $\varepsilon^{\mu}_{//}(H_{surf})$. **Fig. 13d.** $\varepsilon^{\mu}_{\perp}(H_{surf})$ cycles for θ = 60° and different levels of uniaxial tensile stress.

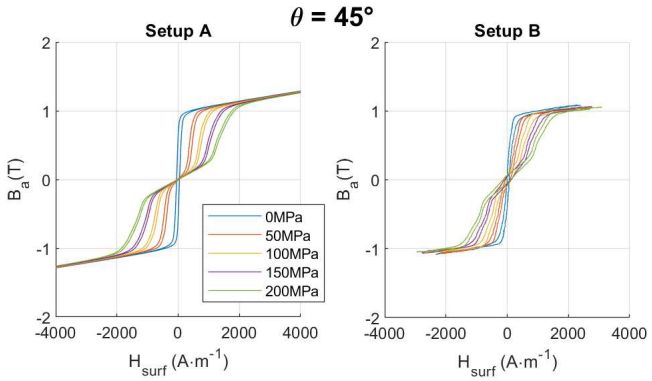

Fig. 14. Comparison between the $B_a(H_{surf})$ hysteresis cycles obtained with the setup A and the setup B for different stress levels.

The stress-strain curve of the tested specimens was not measured in this study, but similar curves on nearly identical specimens for different θ can be found in reference [49].